Inorg. Chem. **2008**, *47*, 10779−10787

Synthesis and Characterization of a Dinuclear Iron(II) Spin Crossover Complex with Wide Hysteresis

Birgit Weber,*,† Eike S. Kaps,† Jaroslava Obel,† Klaus Achterhold,‡ and Fritz G. Parak‡

Ludwig Maximilian University Munich, Department of Chemistry and Biochemistry, Butenandtstr. 5-13 (Haus F), D-81377 München, Germany, and Technische Universität München, Physik-Department E17, James-Franck-Strasse, 85747 Garching, Germany

Received July 24, 2008

The magnetic properties and results from X-ray structure analysis for a new pair of iron(II) spin-crossover complexes $[FeL1(meim)_2](meim)$ (**1**(meim)) and $[Fe_2L2(meim)_4](meim)_4$ (**2**$(meim)_4$), with L1 being a tetradentate $N_2O_2^{2-}$ coordinating Schiff-base-like ligand [([3,3′]-[1,2-phenylenebis(iminomethylidyne)]bis(2,4-pentane-dionato)(2-)-N,N′,O^2,O$^{2′}$], L2 being an octadentate, dinucleating $N_2O_2^{2-}$ coordinating Schiff-base-like ligand [3,3′,3″,3‴]-[1,2,4,5-phenylenetetra(iminomethylidyne)]tetra(2,4-pentanedionato)(2-)*N*,*N*′,*N*″,*N*‴,*O*^{2},*O*$^{2′}$,*O*$^{2″}$,*O*$^{2‴}$], and meim being *N*-methylimidazole, are discussed in this work. Crystalline samples of both complexes show a cooperative spin transition with an approximately 2-K-wide thermal hysteresis loop in the case of **1**(meim) ($T_{1/2↑}$ = 179 K and $T_{1/2↓}$ = 177 K) and an approximately 21-K-wide thermal hysteresis loop in the case of dinuclear complex **2**$(meim)_4$ ($T_{1/2↑}$ = 199 K and $T_{1/2↓}$ = 178 K). For a separately prepared powder sample of **2**, a gradual spin transition with $T_{1/2}$ = 229 K is observed that was additionally followed by Mössbauer spectroscopy. The results from X-ray structure analysis give a deeper insight into the molecule packing in the crystal and, by this, help to explain the increase of cooperative interactions during the spin transition when going from the mononuclear to the dinuclear complex. Both compounds crystallize in the triclinic space group $P\bar{1}$, and the X-ray structure was analyzed before and after the spin transition. The change of the spin state at the iron center is accompanied by a change of the O−Fe−O angle, the so-called bite of the equatorial ligand, from about 109° in the high-spin state to 89° in the low-spin state. The cooperative interactions responsible for the thermal hysteresis loop are due to elastic interactions between the complex molecules in both cases. However, due to the higher symmetry of the dinucleating ligand in **2**$(meim)_4$, a 3D network of short contacts is formed, while for mononuclear complex **1**(meim), a 2D layer of linked molecules is observed. The spin transition was additionally followed in solution using ^{1}H NMR spectroscopy for both complexes. In both cases, a gradual spin transition is observed, and the increase of cooperative interactions when going from the mononuclear to the dinuclear system is solely attributed to the extended network of intermolecular contacts.

Introduction

Spin-transition complexes (spin-crossover, SCO) are an interesting class of compounds that can be switched between two or more states by external perturbations such as temperature, pressure, or light.[1] Several applications in the field of information technology can be envisioned for this class of substance, especially for complexes that exhibit a wide hysteresis around room temperature (memory effect).[2] A key factor for a wide hysteresis is strong cooperative interactions between the metal centers during the spin transition; that means a high efficiency to transmit the geometric and electronic changes that occur during a spin transition from one molecule to another.[3] Different intermoleculear interactions such as π-stacking, hydrogen-bonding, or van der Waals interactions are suitable as information transmitters. However, the spreading of those noncovalent interactions through the crystal is difficult to control.[4] Covalent linkers that lead to polymeric compounds might be a suitable way to avoid this problem.[2a,5]

The investigation of dinuclear SCO complexes as the simplest systems of spin-coupled polymers provides funda-

* Author to whom correspondence should be addressed. Tel.: +49-89218077772. Fax: +49-89218077407. E-mail: bwmch@cup.uni-muenchen.de.
† Ludwig Maximilian University Munich.
‡ Technische Universität München.

10.1021/ic801388a CCC: $40.75
Published on Web 10/21/2008

mental information about intramolecular magnetic interactions and a possible synergy between those interactions and the SCO properties. The possibility to switch those complexes between the three spin-pair states HS−HS, HS−LS and LS−LS (where HS and LS represent the local high-spin and low-spin states of the dinuclear species, respectively) and the potential of extending this switching behavior to larger systems attracted the interest of several research groups.[6] Since the early works of Real et al. on bipyrimidine-bridged iron(II) complexes,[7] several series of new dinuclear iron(II) SCO complexes were reported, and those properties were reviewed recently by Bousseksou et al.[6] Two different SCO processes that lead to stepwise (HS−HS ↔ HS−LS ↔ LS−LS) but also to single-step (HS−HS ↔ LS−LS) transitions were observed. Important achievements are the first example for a one-step HS−HS to LS−LS spin transition[8] and the first "averaged"[9] as well as the first ordered[10] structure of a HS−LS species in a two-step transition. It seems that weak intramolecular interactions are responsible for the direct HS−HS ↔ LS−LS transformation,[11] while a plateau in the $\gamma_{HS} \approx 0.5$ (γ_{HS} = HS molar fraction) region might be either due to the intramolecular energetic stabilization of a HS−LS species[7c,12] that can be confirmed, for example, by Mössbauer spectroscopy[13] or due to intermolecular interactions.[9a] The latter possibility leads to continuous transitions in solution.

Scheme 1. Schematic Representation of the Ligands H_2L1, H_4L2, and meim

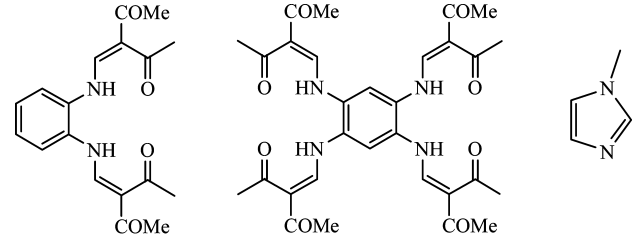

While considerable progress has been made in understanding the two different SCO processes in dinuclear complexes, the question of increasing the cooperative interactions during the spin transition by the use of covalent linkers was eclipsed. To our knowledge, there are only two dinuclear complexes with hysteresis, namely, [{Fe(phdia)$_2$(NCS)$_2$}$_2$(phdia)] (with phdia = 4,7-phenanthroline-5,6-diamine), which shows a stepwise spin transition with a 2- and 7-K-wide hystersis (first and second step, respecitively)[7c] and [(TPyA)Fe(THBQ)Fe(TPyA)](BF$_4$)$_2$ (with TPyA = tris(2-pyridylmethyl)-amine; THBQ = 2,3,5,6-tetrahydroxy-1,4-bbenzoquinonate), which shows a ca. 10-K-wide hysteresis.[14] In this context, we present a pair of complexes where, by application of a dinucleating chelate ligand, the cooperative interactions during the spin transition were increased significantly compared to the mononuclear analogue. In Scheme 1, the general structure of the ligands and the used abbreviations are given. Mononuclear complexes of this ligand type were first investigated by Jäger et al.[15] Gradual and cooperative spin transitions were observed, sometimes even with small hysteresis.[13,16] For the dinuclear complexes of this ligand type, so far only partial spin transitions were observed in the solid state with $\gamma_{HS} > 0.5$.[17] Investigations in solution did show that the incomplete character of the transition curve

(1) (a) Goodwin, H. A. *Coord. Chem. Rev.* **1976**, *18*, 293. (b) Gütlich, P. *Struct. Bonding (Berlin)* **1981**, *44*, 83. (c) König, E. *Prog. Inorg. Chem.* **1987**, *35*, 527. (d) Gütlich, P.; Hauser, A. *Coord. Chem. Rev.* **1990**, *97*, 1. (e) König, E. *Struct. Bonding (Berlin)* **1991**, *76*, 51. (f) Gütlich, P.; Hauser, A.; Spiering, H. *Angew. Chem., Int. Ed. Engl.* **1994**, *33*, 2024, and references therein. (g) Gütlich, P.; Jung, J.; Goodwin, H. *Molecular Magnetism: From Molecular Assemblies to the Devices*; Coronado, 1996; NATO AS I Series E: Applied Sciences; pp 321−327. (h) Gütlich, P.; Goodwin, H. A. Spin Crossover in Transition Metal Compounds I−III. *Topics in Current Chemistry*; Springer-Verlag: New York, 2004. (i) Real, J. A.; Gaspar, A. B.; Munoz, M. C. *Dalton Trans.* **2005**, 2062. (j) Sato, O.; Tao, J.; Zhang, Y.-Z. *Angew. Chem.* **2007**, *119*, 2200; *Angew. Chem. Int. Ed.* **2007**, *46*, 2152−2187.

(2) (a) Kahn, O.; Jay Martinez, C. *Science* **1998**, *279*, 44–48. (b) Kahn, O.; Jay, C.; Kröber, J.; Claude, R.; Grolière, F. U.S. Patent EP0666561, 1995. (c) Létard, J.-F.; Nguyen, O.; Daro, N. U.S. Patent FR0512476, 2005. (d) Létard, J.-F.; Guionneau, P.; Goux-Capes, L. *Topics in Current Chemistry*; Gütlich, P., Goodwin, H. A., Eds.; Springer: NewYork, 2004; Vol. *235*, p 221. (e) Galet, A.; Gaspar, A. B.; Munoz, M. C.; Bukin, G. V.; Levchenko, G.; Real, J. A. *Adv. Mater.* **2005**, *17*, 2949–2953.

(3) Real, J. A.; Gaspar, A. B.; Niel, V.; Munoz, M. C. *Coord. Chem. Rev.* **2003**, *236*, 121–141.

(4) (a) Matouzenko, G. S.; Bousseksou, A.; Lecocq, S.; van Koningsbruggen, P. J.; Perrin, M.; Kahn, O.; Collet, A. *Inorg. Chem.* **1997**, *36*, 5869. (b) Matouzenko, G. S.; Letard, J.-F.; Bousseksou, A.; Lecocq, S.; Capés, L.; Salmon, L.; Perrin, M.; Kahn, O.; Collet, A. *Eur. J. Inorg. Chem.* **2001**, *11*, 2935. (c) Matouzenko, G.; Bousseksou, A.; Borshch, S. A.; Perrin, M.; Zein, S.; Salmon, L.; Molnár, G.; Lecocq, S. *Inorg. Chem.* **2004**, *43*, 227.

(5) (a) Kahn, O.; Codjovi, E. *Philos. Trans. R. Soc. London, Ser. A* **1996**, *354*, 359. (b) Kahn, O.; Garcia, Y.; Létard, J.-F.; Mathoniére, C. *NATO ASI Ser., Ser. C* **1998**, *518*, 127.

(6) Bousseksou, A.; Molnár, G.; Real, J. A.; Tanaka, K. *Coord. Chem. Rev.* **2007**, *251*, 1822–1833, and references therein.

(7) (a) Real, J. A.; Bolvin, H.; Bousseksou, A.; Dworkin, A.; Kahn, O.; Varret, F.; Zarembowitch, J. *J. Am. Chem. Soc.* **1992**, *114*, 4650–4658. (b) Ksenofontov, V.; Spiering, H.; Reiman, S.; Garcia, Y.; Gaspar, A. B.; Moliner, N.; Real, J. A.; Gütlich, P. *Chem. Phys. Lett.* **2001**, *348*, 381–386. (c) Ksenofontov, V.; Gaspar, A. B.; Niel, V.; Reiman, S.; Real, J. A.; Gütlich, P. *Chem.−Eur. J.* **2004**, *10*, 1291–1298. (d) Real, J. A.; Gaspar, A. B.; Munoz, M. C.; Gütlich, P.; Ksenofontov, V.; Spiering, H. *Topics in Current Chemistry*; Gütlich, P., Goodwin, H. A. Springer: NewYork, 2004; Vol. *233*, p 167. (e) Gaspar, A. B.; Munoz, M. C.; Real, J. A. *J. Mater. Chem.* **2006**, 2522–2533.

(8) (a) Leita, B. A.; Moubaraki, B.; Murray, K. S.; Smith, J. P.; Cashion, J. D. *Chem. Commun.* **2004**, *15*, 6–157. (b) Nakano, K.; Suemura, N.; Kawata, S.; Fuyuhiro, A.; Yagi, T.; Nasu, S.; Morimoto, S.; Kaizaki, S. *Dalton Trans.* **2004**, *982*, 988.

(9) (a) Ortega-Villar, N.; Thompson, A. L.; Munoz, M. C.; Ugalde-Sadivar, V. M.; Goeta, A. E.; Moreno-Esparza, R.; Real, J. A. *Chem.−Eur. J.* **2005**, *11*, 5721–5734. (b) Gaspar, A. B.; Ksenofontov, V.; Reiman, S.; Gütlich, P.; Thompson, A. L.; Goeta, A. E.; Munoz, M. C.; Real, J. A. *Chem.−Eur. J.* **2006**, *12*, 9289–9298.

(10) Amoore, J. J. M.; Kepert, C. J.; Cashion, J. D.; Moubaraki, B.; Neville, S. M.; Murray, K. S. *Chem.−Eur. J.* **2006**, *12*, 8220–8227.

(11) Gaspar, A. B.; Ksenofontov, V.; Real, J. A.; Gütlich, P. *Chem. Phys. Lett.* **2003**, *373*, 385–391.

(12) (a) Zein, S.; Borshch, S. A. *J. Am. Chem. Soc.* **2005**, *127*, 16197–16201. (b) Nakano, K.; Kawata, S.; Yoneda, K.; Fuyuhiro, A.; Yagi, T.; Nasu, S.; Morimoto, S.; Kaizaki, S. *Chem. Commun.* **2004**, 2892–2893.

(13) Grunert, M. C.; Reiman, S.; Spiering, H.; Kitchen, J. A.; Brooker, S.; Gütlich, P. *Angew. Chem., Int. Ed.* **2008**, *47*, 2997–2999.

(14) Min, K. S.; Swierczek, K.; Di Pasquale, A. G.; Rheingold, A. L.; Reiff, W. M.; Arif, A. M.; Miller, J. S. *Chem. Commun.* **2008**, 317–319.

(15) (a) Jäger, E.-G. *Chemistry at the Beginning of the Third Millenium*; Fabbrizzi, L., Poggi, A.; Springer Verlag: New York, 2000; Vol. *10*, pp 3−138. (b) Leibeling, G. Ph.D. Thesis, University of Jena/Germany, Jena, Germany, 2003. (c) Müller, B. R.; Leibeling, G.; Jäger, E.-G. *Chem. Phys. Lett.* **2000**, *319*, 368–374.

is due to packing effects.[18] In this work, we present the first dinuclear SCO complex of this ligand type performing a complete spin transition with an over 20-K-wide thermal hysteresis loop.

Experimental Section

Synthesis. If not described differently, all syntheses were carried out under argon using Schlenk tube techniques. All solvents were purified as described in the literature[19] and distilled under argon. The syntheses of the ligands H_2L1,[20] [FeL1(MeOH)$_2$],[21] H_4L2,[22] and iron(II) acetate[23] are described in the literature.

[FeL1(meim)$_2$](meim) (1(meim)) ([3,3′]-[1,2-Phenylenebis(iminomethylidyne)]bis(2,4-pentanedionato)(2-)*N,N′,O*^{2}*,O*$^{2′}$]iron(II)) (N-Methylimidazole)$_3$. FeL1(MeOH)$_2$ (0.47 g, 1.04 mmol) was dissolved in N-methylimidazole (15 mL) and refluxed for half an hour. After cooling, the product was obtained in the form of dark black crystals. The precipitate was filtered off and dried in a vacuum. Yield: 0.14 g (20%). Anal. calcd for $C_{30}H_{36}N_8O_4Fe$ (628.5): C, 57.33; H, 5.77; N, 17.83. Found: C, 57.10; H, 5.80; N, 17.68. IR (Nujol): $\tilde{\nu}$(C=O) = 1635 cm^{-1}. MS (DEI+): base peak, 82 *m*/*z* (100) [meim]; 382 *m*/*z* (60) [FeL1$^+$].

[Fe$_2$L2(MeOH)$_4$] ([3,3′,3″,3‴]-[1,2,4,5-Phenylenetetra(iminomethylidyne)]tetra(2,4-pentanedionato)(2-)*N,N′,N″,N‴,O*^{2}*,O*$^{2′}$*,O*$^{2″}$*,O*$^{2‴}$]diiron(II)) (MeOH)$_4$. Fe(OAc)$_2$ (3.19 g, 18.43 mmol) and H_4L2 (4.91 g, 8.49 mmol) were suspended in methanol (80 mL) and refluxed for 1 h. After cooling, the reddish-brown precipitate was filtered off, washed with methanol (2 × 10 mL), and dried in a vacuum. Yield: 3.50 g (50%). Anal. calcd for $C_{34}H_{46}N_4O_{12}Fe_2$ (814.4): C, 50.14; H, 5.69; N, 6.88. Found: C, 49.83; H, 5.72; N, 6.82. IR (Nujol): $\tilde{\nu}$(C=O) = 1645 cm^{-1}. MS (FAB+): 686 *m*/*z* (20) [Fe$_2$L2$^+$].

[Fe$_2$L2(meim)$_4$] (2) ([3,3′,3″,3‴]-[1,2,4,5-Phenylenetetra(iminomethylidyne)]tetra(2,4-pentanedionato)(2-)*N,N′,N″,N‴,O*^{2}*,O*$^{2′}$*,O*$^{2″}$*,O*$^{2‴}$]diiron(II)) (N-Methylimidazole))$_4$. Fe(OAc)$_2$ (0.25 g, 1.43 mmol) and H_4L2 (0.34 g, 0.57 mmol) were suspended in N-methylimidazole (10 mL) and refluxed for 1 h. After cooling, the dark-brown precipitate was filtered off, washed with methanol (1 × 10 mL), and dried in a vacuum. Yield: 0.1 g (20%). Anal. calcd for $C_{46}H_{54}N_{12}O_8Fe_2$ (1014.7): C, 54.45; H, 5.36; N, 16.56. Found: C, 53.97; H, 5.35; N, 16.74. IR (Nujol): $\tilde{\nu}$(C=O) = 1632 cm^{-1}. MS (FAB+): base peak, 83 *m*/*z* (100) [meim]; 686 *m*/*z* (35) [Fe$_2$L2$^+$]; 768 *m*/*z* (15) [Fe$_2$L2(meim)$^+$]; 850 *m*/*z* (1) [Fe$_2$L2(meim)$_2^+$].

[Fe$_2$L2(meim)$_4$](meim)$_4$ (2(meim)$_4$) ([3,3′,3″,3‴]-[1,2,4,5-Phenylenetetra(iminomethylidyne)]tetra(2,4-pentanedionato)(2-)*N,N′,N″,N‴,O*^{2}*,O*$^{2′}$*,O*$^{2″}$*,O*$^{2‴}$]diiron(II)) (N-Methylimidazole)$_8$). [Fe$_2$L2(MeOH)$_4$] (0.46 g, 0.56 mmol) was suspended in N-methylimidazole (10 mL) and refluxed for 1 h. After cooling, the solution was left to stand overnight to obtain black crystals that were filtered off and dried in a vacuum. Yield: 0.12 g (15%). Anal. calcd for $C_{62}H_{78}N_{20}O_8Fe_2$ (1343.1): C, 55.44; H, 5.85; N, 20.86. Found: C, 55.20; H, 6.16; N, 22.43. IR (Nujol): $\tilde{\nu}$(C=O) = 1650 cm^{-1}. MS (FAB+): 686 *m*/*z* (55) [Fe$_2$L2$^+$]; 768 *m*/*z* (25) [Fe$_2$L2(meim)$^+$]; 850 *m*/*z* (3) [Fe$_2$L2(meim)$_2^+$].

Magnetic Measurements. Magnetic measurements of the samples were performed on a Quantum-Design-MPMSR-XL-SQUID-Magnetometer in a temperature range from 2 to 300 K. All measurements were carried out at two field strengths (0.02 and 0.05 T) in the settle mode. The data were corrected for the magnetization of the sample holder, and diamagnetic corrections were estimated using Pascal's constants.

Mössbauer Spectra. Mössbauer spectra have been recorded using a conventional Mössbauer spectrometer operating in a sinusoidal velocity profile. The sample was placed in a bath cryostat (Cryo Industries of America Inc., Model 11CC).

NMR Spectroscopy. Deuterated chemicals, methanol-d_4 (D, 99.5%) and toluene-d_8 (D, 99.6%), were purchased from Eurisotop. The solvents were degassed with argon and stored over molecular sieves. The NMR samples were prepared under argon using Schlenk techniques and locally made sealing equipment. Saturated solutions of the iron(II) complexes were prepared in a 1 M solution of N-methylimidazole in toluene-d_8/methanole-d_4 mixtures (50/50 v/v %) and stored in sealed or airtight 5 mm NMR tubes. The NMR spectra were recorded on a JEOL EX 400e spectrometer operating at 400.182 MHz equipped with a variable-temperature unit over the temperature range −80 to +60 °C.

Crystal Structure Analysis. The intensity data for the both complexes were collected on an *Oxford XCalibur* diffractometer using graphite monochromated Mo Kα radiation. Data were corrected for Lorentz and polarization effects. The structures were solved by direct methods (Sir 97)[24] and refined by full-matrix least-squares techniques against F_0^2 (SHELXL-97).[25] The hydrogen atoms were included at calculated positions with fixed thermal parameters. All nonhydrogen atoms were refined anisotropically. Cell parameters and refinement results for all complexes are summarized in Table 1. ORTEP-III was used for structure representation.[26] The quality of the data of **2**(meim)$_4$ in the HS state is inferior. We will therefore only be publishing the conformation of the molecule and the crystallographic data.

Results and Discussion

Synthesis. The ligand H_2L1,[20] the dinucleating ligand H_4L2,[22] and [FeL1(MeOH)$_2$][21] were prepared as reported previously. Crystals of the mononuclear complex **1**(meim) were synthesized by dissolving [FeL1(MeOH)$_2$] in N-methylimidazole at 80 °C followed by slow crystallization. The synthesis of a powder sample of complex **1** and its magnetic properties were reported previously.[16c] The powder sample of **2** was obtained by the conversion of iron(II) acetate with H_4L2 in N-methylimidazole. Crystals of **2**(meim)$_4$ were obtained by dissolving [Fe$_2$L2(MeOH)$_4$] in N-methylimidazole at 80 °C followed by slow crystallization. Grinding of

(16) (a) Weber, B.; Kaps, E.; Weigand, J.; Carbonera, C.; Letard, J.-F.; Achterhold, K.; Parak, F.-G. *Inorg. Chem.* **2008**, *47*, 487–496. (b) Weber, B.; Carbonera, C.; Desplanches, C.; Létard, J.-F. *Eur. J. Inorg. Chem.* **2008**, *158*, 9–1598. (c) Weber, B.; Kaps, E. S.; Obel, J.; Bauer, W. *Z. Anorg. Allg. Chem.* **2008**, 1421–1426. (d) Weber, B.; Kaps, E. S.; Desplanches, C.; Létard, J.-F.; Achterhold, K.; Parak, F. G. *Eur. J. Inorg. Chem.* DOI: 10.1002/ejic.200800420.
(17) Weber, B.; Kaps, E. *Heteroatom Chem.* **2005**, *16*, 391–397.
(18) Weber, B.; Walker, F. A. *Inorg. Chem.* **2007**, *46*, 6794–6803.
(19) *Autorenkollektiv: Organikum*; Johann Ambrosius Barth Verlagsgesellschaft mbH: Germany, 1993.
(20) Wolf, L.; Jäger, E.-G. *Z. Anorg. Allg. Chem.* **1966**, *346*, 76.
(21) Jäger, E.-G.; Häussler, E.; Rudolph, M.; Schneider, A. *Z. Anorg. Allg. Chem.* **1985**, *525*, 67.
(22) Hasty, E. F.; Colburn, T. J.; Hendrickson, D. N. *Inorg. Chem.* **1973**, *12*, 2414–2421.
(23) Heyn, B.; Hipler, B.; Kreisel, G.; Schreer, H.; Walter, D. *Anorganische Synthesechemie*; Springer Verlag: Heidelberg, Germany, 1986.
(24) Altomare, A.; Burla, M. C.; Camalli, G. M.; Cascarano, G.; Giacovazzo, C.; Guagliardi, A.; Moliterni, A. G. G.; Polidori, G.; Spagna, R. *J. Appl. Crystallogr.* **1999**, *32*, 115; *SIR 97*, Campus Universitario Bari: Bari, Italy, 1997.
(25) Sheldrick, G. M. *SHELXL 97*; University of Göttingen: Göttingen, Germany, 1993.
(26) (a) Johnson, C. K.; Burnett, M. N. *ORTEP-III*; Oak-Ridge National Laboratory: Oak Ridge, TN, 1996. (b) Farrugia, L. J. *J. Appl. Crystallogr.* **1997**, *30*, 565.

Table 1. Crystallographic Data for Octahedral Iron(II) Complexes Discussed in This Work

	1(meim) (HS)	**1**(meim) (LS)	**2**(meim)$_4$ (HS)	**2**(meim)$_4$ (HS/LS)	**2**(meim)$_4$ (LS)
formula	$C_{30}H_{36}FeN_8O_4$	$C_{30}H_{36}FeN_8O_4$	$C_{62}H_{78}Fe_2N_{20}O_8$	$C_{62}H_{78}Fe_2N_{20}O_8$	$C_{62}H_{78}Fe_2N_{20}O_8$
fw, g·mol^{-1}	628.503	628.503	1343.102	1343.102	1343.102
cryst syst	triclinic	triclinic	triclinic	triclinic	triclinic
space group	$P\bar{1}$	$P\bar{1}$	$P\bar{1}$	$P\bar{1}$	$P\bar{1}$
a (Å)	11.781(3)	11.676(3)	10.3699(4)	10.144(2)	10.054(3)
b (Å)	11.905(5)	11.7660(14)	13.8647(6)	13.415(3)	13.352(3)
c (Å)	11.951(2)	11.8250(17)	14.1602(8)	13.869(4)	13.825(4)
α (deg)	73.24(3)	77.356(11)	64.421(5)	114.21(2)	114.54(2)
β (deg)	78.18(2)	72.901(17)	68.253(4)	109.45(2)	109.45(3)
γ (deg)	73.33(3)	72.642(10)	88.582(3)	91.36(2)	91.78(2)
V (Å^3)	1523.8(8)	1466.6(5)	1683.29(13)	1594.6(7)	1560.6(9)
Z	2	2	1	1	1
d_{calcd} (g·cm^{-3})	1.37	1.42	1.313	1.399	1.4291
μ (mm^{-1})	0.544	0.565	0.498	0.526	0.538
Θ range, deg	3.79−24.99	3.75−23.50	3.73−23.25	3.73−24.25	3.76−24.25
λ, Å	0.71073	0.71073	0.71073	0.71073	0.71073
T, K	250(2)	135(2)	300(2)	200(2)	125(2)
GOF	0.993	1.008	1.909	0.961	1.095
R1,[a] wR2[b] ($I > 2\sigma(I)$)	0.0389, 0.1068	0.0444, 0.1205	0.1299, 0.4295	0.0515, 0.1460	0.0517, 0.1513

[a] $R1 = \sum||F_o| - |F_c||/\sum|F_o|$. [b] $wR2 = [\sum[w(F_o^2 - F_c^2)^2]/\sum w(F_o^2)^2]^{1/2}$, $w = 1/[\sigma^2(F_o^2) + (aP)^2 + bP]$, where $P = [F_o^2 + 2(F_c^2)]/3$.

the crystals of **2**(meim)$_4$ and heating of those pulverized crystals to 100 °C in a vacuum is an alternative way to yield the powder sample of **2**.

Magnetic Properties. The thermal dependence of the product $\chi_M T$ (χ_M being the molar susceptibility and T the temperature) for **1**(meim) (triangles) is displayed on the top of Figure 1. For comparison, the results for the powder sample of **1**[16c] are included as well (open circles). The room temperature value, $\chi_M T = 3.35$ cm^3 K mol^{-1}, of the crystalline sample is within the range expected for a mononuclear iron(II) complex in the HS state. Upon cooling, an abrupt HS ↔ LS transition is observed in the region between 182 and 172 K. The characteristic temperature $T_{1/2}$ (with the HS molar fraction $\gamma_{HS} = 0.5$) is 177 K in the cooling mode and 179 K in the heating mode; a 2-K-wide thermal hysteresis loop is observed. In the low-temperature region of the spectrum, all iron centers are essentially in the LS state with $\chi_M T = 0.02$ cm^3 K mol^{-1} at 100 K. The plot of $\chi_M T$ versus the temperature for the different samples of dinuclear complex **2** is given in the bottom of Figure 1. The powder sample of **2** (open circles) performs a gradual spin transition in the temperature region of 275−175 K. The room temperature value ($\chi_M T = 5.98$ cm^3 K mol^{-1}) is in the region expected for a dinuclear iron(II) complex with both iron centers essentially in the HS state. The transition is centered at 229 K, and no thermal hysteresis is observed. If the complex [Fe_2L2(MeOH)$_4$] is used as a starting material for the formation of compound **2** instead of a one-pot reaction where the free ligand, iron(II) acetate, and N-methylimidazole are converted in one step, a polycrystalline sample of **2**(meim)$_4$ is obtained. The plot of $\chi_M T$ versus T (open triangles in Figure 2) shows a cooperative spin transition at lower temperatures. The room temperature value ($\chi_M T = 5.91$ cm^3 K mol^{-1}) is in the same region as that found for the powder sample of **2**. Upon cooling, the $\chi_M T$ product decreases first slowly, then more and more rapidly, until at 180 K about 50% of the iron centers are in the LS state. Below this point, the remaining HS iron centers perform a step transition into the LS state with $\chi_M T = 0.38$ cm^3 K mol^{-1} at 100 K. Upon heating, the $\chi_M T$ product remains constant until 195 K, where a step transition into the HS state takes place with about 75% of the iron centers involved. After this step, the $\chi_M T$ product slowly increases further along the cooling curve until the starting value of 5.91 cm^3 K mol^{-1} is reached at room temperature. The critical temperatures are 178 K upon cooling and 199 K upon heating, corresponding to a 21-K-wide thermal hysteresis loop.

Due to the incomplete character of the spin transition of the dinuclear complexes in the high-temperature region, it is difficult to determine the exact value of the HS molar fraction for the different temperatures. Therefore, the spin transition of the powder sample of **2** was additionally followed using Mössbauer spectroscopy in the temperature region 80−300 K in the heating mode. Selected spectra at different temperatures are given in Figure 2 with the HS mole fraction indicated. Values of the Mössbauer parameters obtained by least-squares fitting of the spectra are gathered in the Supporting Information, Table S1. At 80 K, the Mössbauer spectrum consists of a unique quadrupole-split doublet, with an isomer shift of 0.48 mm/s and a quadrupole splitting of 1.08 mm/s. These parameters are typical for LS iron(II). Above 190 K, a HS iron(II) doublet appears with the parameters $\delta = 0.98$ mm/s and $\Delta E = 2.26$ mm/s at 280 K. No evidence of a residual HS fraction is found in the low-temperature region; however, at 300 K, the spin transition is still not complete. The high-spin mole fraction γ_{HS} at each temperature was deduced from the area ratio A_{HS}/A_{tot} determined from the least-squares fitting of the spectra (A_{HS} = area of the HS doublet; A_{tot} = total Mössbauer absorption) and corrected by the Lamb Mössbauer factor. A complete description of the procedure is given in the Supporting Information. At 300 K, a value of $\gamma_{HS} = 0.88$ is obtained. About 10% of the molecules are still in the LS state. This is in good agreement with the results from the susceptibility measurements.

For a better comparison, the intermolecular interaction parameter Γ was determined using the mean-field model

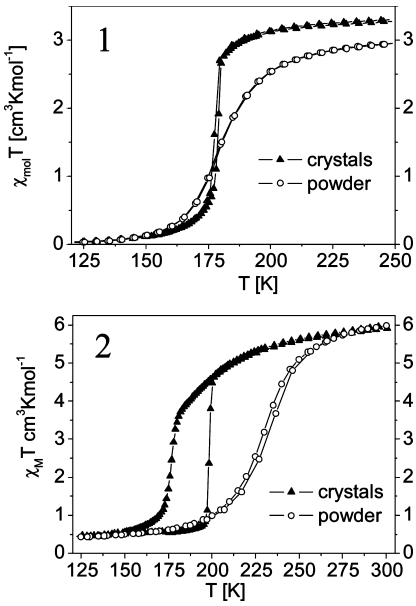

Figure 1. Plot of the $\chi_M T$ product vs T for different samples of compounds **1** (top) and **2** (bottom). Full triangles: crystalline samples of **1**(meim) and **2**(meim)$_4$. Open circles: powder samples of **1** and **2**.

proposed by Slichter and Drickamer.[27] In this model, the temperature dependence of the HS molar fraction γ_{HS} is given through eq 1, where ΔH_{HL} and ΔS_{HL} are the entropy and enthalpy changes associated with the spin transition, Γ is the intermolecular interaction parameter, and f_{HS} corresponds to the remaining HS molar fraction.

$$\ln\left(\frac{1-\gamma_{HS}}{\gamma_{HS}-f_{HS}}\right)=\frac{\Delta H_{HL}+\Gamma(f_{HS}+1-2\gamma_{HS})}{RT}-\frac{\Delta S_{HL}}{R} \quad (1)$$

This was done by least-squares fittings of the γ_{HS} (HS molar fraction) versus T curves of the different samples of the two complexes. The obtained fitting parameters are given in Table 2. In the Supporting Information, Figures S1 and S2, the fit of γ_{HS} versus T is represented for the different samples of the two complexes with the used parameters indicated. Due to the complex curve progression, for compound **2**(meim)$_4$, only a simulation of the spin transition curve was possible using the ΔH_{HL} and ΔS_{HL} values of the powder sample as a starting point. The obtained ΔH_{HL} and ΔS_{HL} values of all complexes are in the range expected for iron(II) spin-crossover complexes.[1] For the mononuclear complex, the values are on the same order of magnitude as reported previously for SCO complexes of this ligand type.[14] Following the suggestion of Purcell and Edwards,[28] the parameter C ($= \Gamma/2RT_{1/2}$ = cooperativity factor) was determined. Its value increases from **2** (0.63) to **1** (0.85) to **1**(meim) (1.11) to **2**(meim)$_4$ (1.56) and clearly reflects the increasing width of the hysteresis of the different samples. Interestingly, the cooperativity factor of the powder sample of **1** is with $C = 0.85$ larger than that for the powder sample of **2**, while for the crystalline samples, an opposite order is obtained. This observation indicates that the covalent bridge

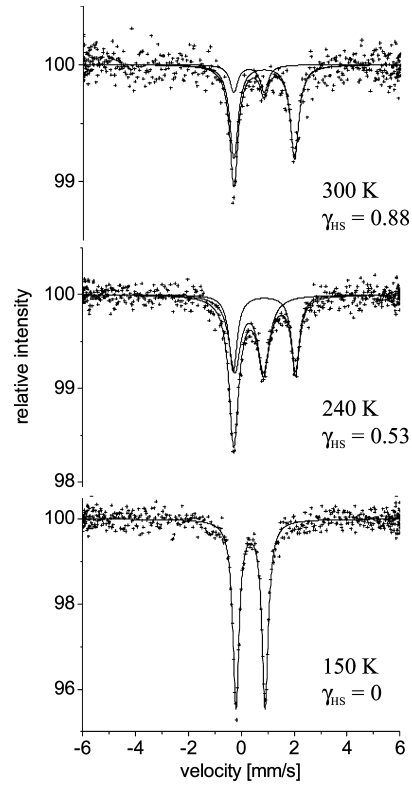

Figure 2. Plot of the Mössbauer spectra of compound **2** at 150, 240, and 300 K with the high-spin molar fraction indicated.

Table 2. Least-Squares Fitting Parameters for the Complexes Using the Mean-Field Model Proposed by Slichter and Drickamer (eq 1)[25]

complex	ΔH_{HL} [kJ mol^{-1}]	ΔS_{HL} [J mol^{-1}K^{-1}]	$T_{1/2}$ [K]	Γ [kJ mol^{-1}]	C
1[a]	8.01±0.06	43.9±0.3	183	2.60±0.03	0.85
1(meim)	7.24±0.22	40.9±1.2	177	3.27±0.04	1.11
2	16.6 ±2.5	72.4±9.9	229	2.4 ±0.7	0.63
2(meim)$_4$	14.88	77.9	191	4.95	1.56

[a] From ref 14c.

of the dinuclear complex has little or no influence on the cooperative interactions during the spin transition. The different hysteresis widths must therefore correlate with the packing of the molecules in the crystal and the intermolecular interactions.

X-Ray Structure Analysis. Crystals suitable for X-ray structure analysis have been obtained for the two crystalline compounds **1**(meim) and **2**(meim)$_4$. Selected bond lengths and angles within the first coordination sphere are summarized in Table 3. The crystallographic data of the complexes are summarized in Table 1. Ortep drawings of the HS form of **1**(meim) and the LS form of **2**(meim)$_4$ are given in Figures 3 and 4 with the atom numbering schema indicated. In both cases, it was possible to determine the X-ray structure before and after the spin transition; however, for the room temperature structure of **2**(meim)$_4$, the quality of the data was inferior, probably because of a high disorder of the included methylimidazole molecules. Only the conformation of the molecule will be discussed.

Intramolecular Changes during the Spin Transition. The average bond lengths are 2.09 Å (Fe−N_{eq}), 2.02 Å (Fe−O_{eq}), and 2.26 Å (Fe−N_{ax}) in the HS state and 1.90 Å (Fe−N_{eq}), 1.94 Å (Fe−O_{eq}), and 2.01 Å (Fe−N_{ax}) in the LS

(27) Slichter, C. P.; Drickamer, H. G. *J. Chem. Phys.* **1972**, *56*, 2142–2160.
(28) Purcell, K. F.; Edwards, M. P. *Inorg. Chem.* **1984**, *23*, 2620–2625.

Table 3. Selected Bond Lengths [Å] and Angles [deg] within the First Coordination Sphere of the Iron(II) Complexes Discussed in This Work with Spin State S

complex	T [K]	S	Fe−N1/2	Fe−O1/2	Fe−N3/4	O1−Fe−O2	N_{ax}−Fe−N_{ax}	∠L1, L2[a]
1(meim)	250	2	2.077(2)	1.999(2)	2.250(3)	106.84(7)	179.24(8)	59.64
			2.083(2)	2.009(2)	2.279(2)			
1(meim)	135	0	1.892(3)	1.934(2)	2.011(3)	88.40(9)	178.95(10)	56.49
			1.899(3)	1.940(2)	2.016(3)			
2(meim)$_4$	300	2	2.09	2.04	2.25	108	177	45.52
2(meim)$_4$	200		1.920(3)	1.937(2)	2.039(3)	90.25(11)	178.26(12)	43.79
			1.925(3)	1.949(3)	2.054(3)			
2(meim)$_4$	125	0	1.902(3)	1.933(2)	2.003(3)	88.24(9)	178.07(10)	44.22
			1.904(3)	1.944(2)	2.023(3)			

[a] Angle between the planes of the axial ligands.

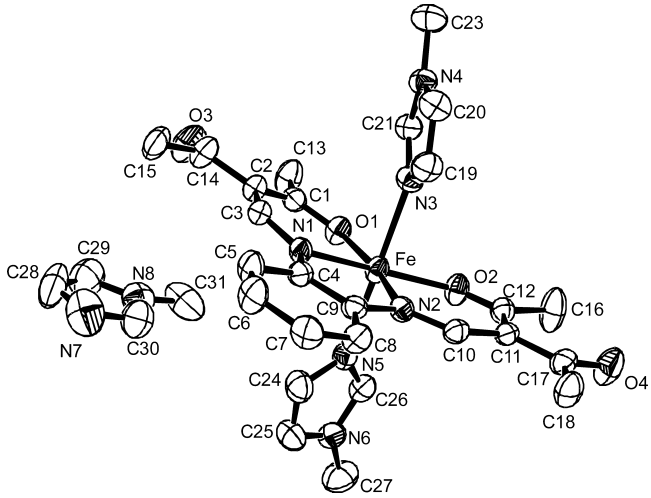

Figure 3. Ortep drawing of the asymmetric unit of **1**(meim) in the HS form showing the 50% probability ellipsoids with the atom numbering scheme used in the text. The hydrogen atoms have been omitted for clarity.

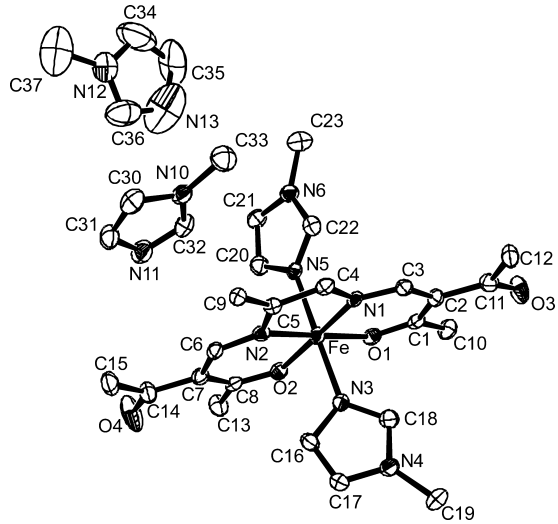

Figure 4. Ortep drawing of the asymmetric unit of **2**(meim)$_4$ in the LS form showing the 50% probability ellipsoids with the atom numbering scheme used in the text. The hydrogen atoms have been omitted for clarity.

state. They are in the same region as found for previously published mononuclear and dinuclear complexes of the same ligand type.[15−17] The shortening of the bond lengths upon spin transition is in the region of about 10%, as discussed for other iron(II) spin-crossover complexes in the literature.[1] The O−Fe−O angle of this type of complex, the so-called bite of the ligand, is a characteristic feature for determining

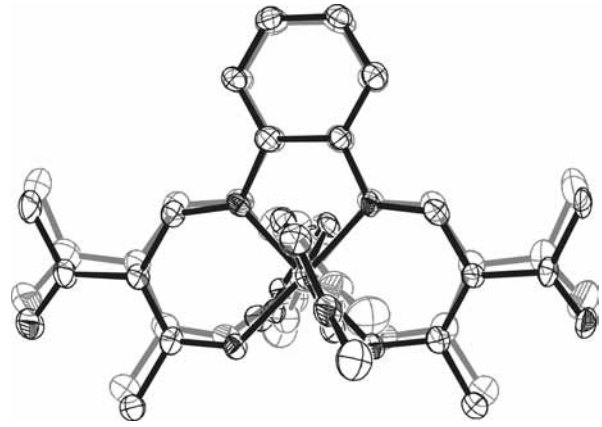

Figure 5. Schematic drawing of the top view of both HS and LS forms of **1**(meim). The molecule at $T \cong 135$ K is the upper one. Fe−N(1,2) bonds are superimposed. The change in the O−Fe−O angle (HS, 106.8°; LS, 88.4°) is clearly visible. Hydrogen atoms and the additional meim molecule have been omitted for clarity.

Table 4. Selected Intermolecular Distances of **1**(meim) at 250 K/135 K[a]

contact	H···A [Å]	D···A [Å]	D−H···A [deg]
C(20)−H(20)···N(7)[b]	2.576/2.561	3.447/3.432	156.1/156.1
C(23)−H(23)···O(2)[c]	2.555/−	3.387/−	145.1/−
C(31)−H(31)···O(4)[c]	2.457/2.516	3.379/3.443	160.8/162.1
C(27)−H(27)···O(3A)[d]	2.343/2.411	3.196/3.301	147.6/154.3
H(6)···H(16)[e]	2.276/2.219		
H(15)···H(28)[f]	2.316/−		
H(27)···H(31)[f]	2.175/2.252		
H(15)···C(7)[c]	−/2.832		

[a] Only contacts shorter than the sum of the van der Waals radii −0.05 Å are considered. [b] $-1+x, 1+y, z$. [c] $1-x, 1-y, 1-z$. [d] $1-x, y, z$. [e] $x, y, 1+z$. [f] $-1+x, y, z$.

the spin state of the iron center. It changes from an average of 107° in the HS state to an average of 88° in the LS state. A schematic drawing of the top view of both, the HS and the LS form, is given in Figure 5 for the mononuclear complex **1**(meim) to illustrate the differences. The change in the cell volume of **1**(meim) ($\Delta V/V = 3.8\%$, $\Delta V = 28.7$ Å^3/Fe) is in the region expected for iron(II) spin-crossover complexes ($\Delta V/V = 3.8-6\%$; $\Delta V = 25-35$ Å/Fe[1]), in good consistence with the values of previously published complexes of this ligand type.[14] In the case of the dinuclear compound **2**(meim)$_4$ ($\Delta V/V = 7.6\%$, respectively $\Delta V = 61.4$ Å^3/Fe), a significantly higher cell volume change is observed. This can be associated with the strong cooperative interactions during the spin transition.

Selected intermolecular distances are reported in Table 4 for **1**(meim) and Table 5 for **2**(meim)$_4$. An extract of the molecule packing of **1**(meim) and **2**(meim)$_4$ is given in the

Table 5. Selected Intermolecular Distances of **2**(meim)$_4$ at 125 K[a]

Contact	H···A [Å]	D···A [Å]	D−H···A [deg]
C(19)−H(19)···O(3)[b]	2.542	3.474	163.9
C(22)−H(22)···O(4)[c]	2.468	3.282	146.3
C(30)−H(30)···O(3)	2.480	3.333	152.5
C(37)−H(37)···N(11)	2.552	3.295	134.4
H(19)···O(2)[d]	2.605		
H(15)···N(11)[e]	2.665		
H(19)···H(35)[d]	2.313		
C(30)···H(36)[f]	2.723		

[a] Only contacts shorter than the sum of the van der Waals radii −0.05 Å are considered. [b] $1-x, -y, 1-z$. [c] $1+x, y, z$. [d] $-x, -y, 1-z$. [e] $x, y, 1+z$. [f] $1-x, 1-y, 1-z$.

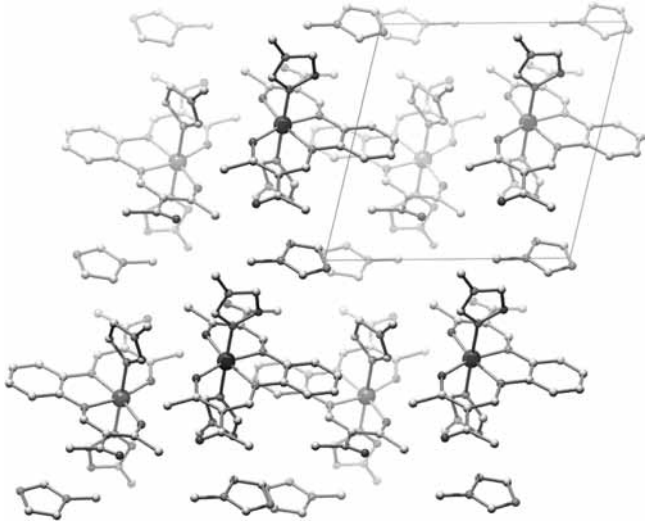

Figure 6. Packing of the molecules of **1**(meim) in the crystal at 250 K projected along [0 0 1].

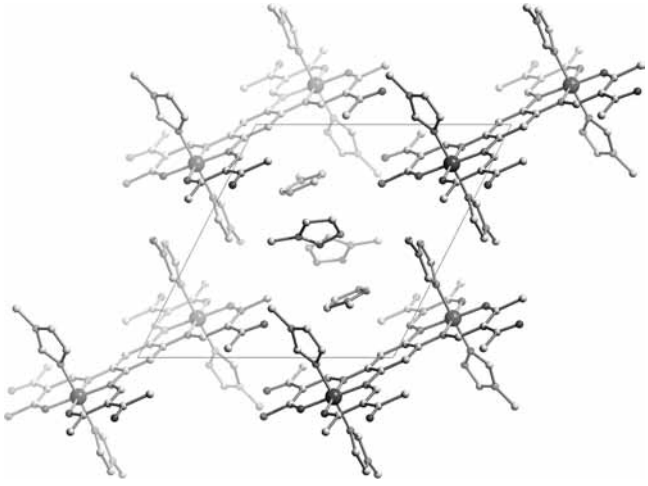

Figure 7. Packing of the molecules of **2**(meim)$_4$ in the crystal at 125 K projected along [1 0 0].

Figures 6 and 7, respectively. On first view, one might assume that both complexes should show a similar degree of cooperative interactions, as in Tables 4 and 5 approximately the same number of short contacts can be found. If elastic interactions between the molecules are made responsible for transmitting the geometric changes occurring during the spin transition, similar hysteresis loops should be expected for the two compounds. For both complexes, there are two contacts of the type C−H···A (with A = O or N; weak or nonclassical hydrogen bonds) that directly link the complex molecules. Some additional contacts mediated over the included methylimidazole molecules can be found as further C···H or H···H van der Waals contacts. If all of the contacts are considered, for both complexes, a 3D network of linked molecules is obtained. The assumption that the hydrogen-bond-like contacts have a higher impact on the cooperative interactions leads in the case of **1**(meim) to a 2D layer of linked molecules. For the dinuclear complex, however, the fact has to be considered that the contacts listed in Table 5 belong to the asymmetric unit, and the whole complex molecule is obtained when the inversion center in the middle of the phenylene bridge is used to generate the second half. This means that, for the whole molecule, twice the number of intermolecular contacts per molecule are obtained compared to the mononuclear analogue. Instead of a 2D network of hydrogen-bond-like contacts for **2**(meim)$_4$, a 3D network is obtained. Those two points together, the duplication of the number of contacts and the increased dimension of the hydrogen-bond-like network, satisfactorily explain the significantly higher cooperative interactions for the dinuclear complex.

For the mononuclear complex **1**(meim), an elongation for most of the intermolecular distances is observed upon cooling. As a consequence, the intensity of the contacts decreases, although the number of relevant contacts remains constant. This gives a good explanation for the more gradual character of the transition curve in the second part of the spin transition. The discontinuous character of the transition curve of crystalline sample **2**(meim)$_4$ is probably due to an order−disorder transition of the included meim molecules in the crystal. A similar behavior was previously reported for two complexes of the formula $[FeL_2](A)_2$ with L = 2,6-di(3-methylpyrazol-1-yl)pyrazine and A = BF_4^- or ClO_4^-, where an order−disorder transition of the counteranions controls the course of the spin transition.[29] In order to prove this theory, the cell parameters of a single crystal of **2**(meim)$_4$ were determined as function of the temperature in the heating and cooling mode. The results are summarized in Table 6.

The spin transition of **2**(meim)$_4$ is accompanied by a significant change of the cell parameters. At 200 K, the temperature where the thermal hysteresis loop starts, cell parameters typical for the LS form are determined, while at higher temperatures, different parameters are obtained that strongly depend on the temperature. This is an indication for an order−disorder transition, most likely of the at-room-temperature disordered meim in the crystal packing, around 200 K. This change could be responsible for the change in the transition curve from a gradual to abrupt with hysteresis. Consequently, the X-ray structure was determined at 200 K, and the results are included in Tables 1 and 3. Indeed, at 200 K, both of the additional meim molecules are ordered. The 50% probability ellipsoids of the formerly disordered meim are more pronounced, indicating that the disorder did not completely freeze out at this temperature. The structure of the iron complex shows no significant differences aside from those caused by mixed HS/LS state. The transition from

(29) Money, V. A.; Elhaik, J.; Evans, I. R.; Halcrow, M. A.; Howard, J. A. K. *Dalton Trans.* **2004**, 65–69.

Table 6. Cell Parameters of **2**(meim)$_4$ in Dependence on Temperature in the Heating and Cooling Mode

T [K]	a (Å)	b (Å)	c (Å)	α (deg)	β (deg)	γ (deg)	V (Å^3)
300 ↓	10.3699(4)	13.8647(6)	14.1602(8)	64.421(5)	68.253(4)	88.582(3)	1683.29(13)
250 ↓	10.327(8)	13.873(10)	14.085(11)	64.34(8)	68.82(7)	88.58(6)	1675(2)
200 ↓	10.144(2)	13.415(3)	13.869(4)	114.21(2)	109.45(2)	91.36(2)	1594.6(7)
180 ↓	10.131(10)	13.386(17)	13.909(16)	114.32(12)	109.63(10)	91.42(9)	1589(3)
170 ↓	10.118(10)	13.384(18)	13.909(16)	114.45(12)	109.62(9)	91.45(9)	1585.29(10)
125 ↓	10.054(3)	13.352(3)	13.825(4)	114.54(2)	109.45(3)	91.78(2)	1560.6(9)
190 ↑	10.145(11)	13.389(16)	13.918(17)	114.37(12)	109.66(10)	91.29(9)	1593(3)
200 ↑	10.163(11)	13.400(16)	13.921(17)	114.26(11)	109.71(10)	91.20(9)	1598.7(1)
210 ↑	13.43(1)	10.18(1)	23.57(2)	88.92(7)	94.53(8)	88.87(8)	3210.4(1)
220 ↑	13.86(1)	14.11(1)	20.13(2)	71.28(7)	71.67(7)	65.64(8)	3318(4)

one meim molecule being disordered to both being ordered is responsible for the complex curve progression of the spin transition of **2**(meim)$_4$.

Investigations in Solution Using ^{1}H NMR Spectroscopy. Variable-temperature NMR spectroscopy is a valuable tool to follow a spin transition in solution by interpretation of the temperature dependence of the ^{1}H NMR chemical shifts.[18] In order to prove the influence of the phenylene bridge on the spin transition of **2** compared to **1**, both complexes were dissolved in a 1 M solution of methylimidazole in d^8-toluene/d^4-methanol (50/50 v/v %). The iron center was assumed to retain its octahedral coordination sphere; however, all packing effects are switched off. The signal assignment and the interpretation of the temperature dependence of the chemical shifts were performed using the same procedures as published previously.[18,16b] All experimental details including the fitting procedures with the TDF (temperature-dependent fitting) program written by Shokhirev and Walker[30] are summarized in the Supporting Information, Figures S7 and S8 and Table S2. In Figure 8, the transition curves obtained in solution are compared with the results from SQUID measurements in the solid state for both complexes.

Due to the low transition temperature for both complexes in solution, only the beginning of the spin transition could be detected using solution ^{1}H NMR spectroscopy. Nevertheless, some trends can be observed. For the mononuclear complex, the transition curve obtained in solution is very similar to the one obtained for the powder sample, and similar $T_{1/2}$ values can be expected. In contrast to this, for the dinuclear complex, the spin transition in solution is more similar to the beginning of the transition curve of the crystalline sample **2**(meim)$_4$. Assuming a gradual spin transition in solution, the $T_{1/2}$ value would be in a similar region as obtained for the mononuclear complex. Indeed, the transition curves of the mononuclear and the dinuclear complex in solution are very similar. This is in agreement with observations made for pyridine adducts of the same ligand type, where no indication for an increase of cooperative interactions can be found in solution when going from the monomer to the dimer complex, and very similar transition curves are obtained.[18] The results obtained for the dinuclear complex demonstrate that not only the extent of cooperative interactions but also the transition temperature can be influenced significantly by packing effects.

Conclusion

The synthesis and characterization of a new pair of SCO complexes is presented in this work. The crystalline samples of both complexes show cooperative spin transitions with a 2- and 21-K-wide hysteresis for the mononuclear and the dinuclear complex, respectively. For the powder samples, gradual spin transitions are observed. Results from X-ray structure analysis indicate that the number and intensity of short intermolecular contacts is responsible for the cooperative nature of the spin transition. In the case of mononuclear complex **1**, a 2D layer of hydrogen-bond-like contacts is observed, while for dinuclear complex **2**, a 3D network is formed. This is due to the higher symmetry of the dinucleating chelate ligand L2 that was prepared by using 1,2,4,5-tetraaminobenzen (D_{2h} symmetry) instead of *o*-phenylenediamine (C_{2v} symmetry). The discontinuous spin transition of dinuclear complex **2** could be traced back to an order−disorder transition of the additional meim molecule in the crystal packing. This pair of complexes is an example of successful crystal engineering where the ligand system was changed to optimize the extent of intermolecular interactions, and by this the desired properties (wide thermal hysteresis loop) are improved. The spin transition of the two complexes was additionally followed in solution by interpreting the ^{1}H NMR shifts. Here, for both samples, gradual spin transitions are obtained, confirming one more time that the

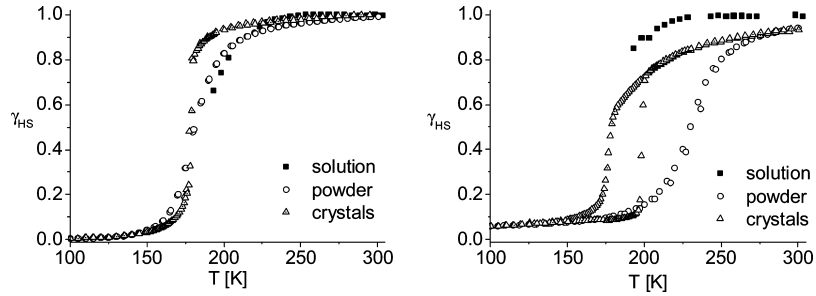

Figure 8. γ_{HS} versus T curves for different samples of the mononuclear (left) and the dinuclear (right) complex followed in solution (full squares) and in the solid state (open circles and open triangles for the powder and the crystalline sample, respectively).

different extent of cooperative interactions can be traced back solely to the extent of the intermolecular contacts.

Acknowledgment. This work has been supported financially by the Deutsche Forschungsgemeinschaft (SPP 1137), the Fonds der Chemischen Industrie, and the Center for Integrated Protein Science Munich (CIPSM).

Supporting Information Available: The thermal variation of γ_{HS} for the four complexes **1**(meim), **1**, **2**(meim)$_4$, and **2** with the least-squares fitting results and the used parameters indicated; the details for the analysis of the Mössbauer spectra together with the least-squares-fitted Mössbauer data (Table S1 and Figures S3−S6); the details for the analysis of the NMR data (Table S2 and Figure S7 and S8); and the crystallographic information files (CIF) of **1**(meim) (250 and 135 K) and **2**(meim)$_4$ (125 and 200 K). This material is available free of charge via the Internet at http://pubs.acs.org.

IC801388A

(30) Shokhirev, N. V.; Walker, F. A. Temperature-Dependent Fitting. http://www.shokhirev.com/nikolai/programs/prgsciedu.html (accessed Sep 2008).